Advanced Functional Materials

Self-assembled pH-Sensitive Fluoro-Magnetic Nanotubes as Archetype System for Multimodal Imaging of Brain Cancer

--Manuscript Draft--

Manuscript Number:	adfm.201707582R1
Full Title:	Self-assembled pH-Sensitive Fluoro-Magnetic Nanotubes as Archetype System for Multimodal Imaging of Brain Cancer
Article Type:	Full Paper
Section/Category:	
Keywords:	multifunctional probes self-assembled nanomaterials fluoro-magnetic nanotubes cancer imaging blood brain barrier
Corresponding Author:	Angelo Monguzzi, Ph.D. Universita degli Studi di Milano-Bicocca Milano, ITALY
Additional Information:	
Question	**Response**
Please submit a plain text version of your cover letter here. **If you are submitting a revision of your manuscript, please do not overwrite your original cover letter. There is an opportunity for you to provide your responses to the reviewers later; please do not add them here**.	Dear Dr. Li, This letter is aimed to present the revised version of the manuscript adfm.201700951 that we submitted to Advanced Functional Materials several months ago. That manuscript has been not considered for publication according to the Referees comments that, despite a general positive judgement, pointed out the lack of several evidences of the potential effective use of the material proposed, i.e. pH-sensitive fluoro-magnetic nanotubes (FluoroMags) for the imaging of brain cancer, for in vivo applications. Taking inspiration from the comments received, we performed additional experiments in order to demonstrate the validity of our material as archetype system for the development of multifunctional probes for brain cancer imaging. I deeply apologize for the delay of this email, but in vivo experiments are really time consuming and requires a lot of efforts and transversal competences. However, we are confident that you will appreciate our results that answer to the Referees' concerns, as detailed in the attached supporting information file. Therefore, we are submitting a revised version of the manuscript, now titled "Self-assembled ph-Sensitive Fluoro-Magnetic Nanotubes as Archetype System for Multimodal Imaging of Brain Cancer" for your consideration in Advanced Functional Materials. In this work, we demonstrate how to fabricate, by means of an ionic self-assembly strategy, fluoro-magnetic chrysotile nanotubes that can serve as multimodal probes for the imaging and targeting of the brain cancer. Their ferromagnetic properties make them suitable contrast agents for magnetic resonance imaging in living animals, while the pH-sensitiveness of their organic component enables to follow the disease evolution by mapping the acidic carcinogenic environment through fluorescence microscopy. In order to experimentally validate this newfound motif, the material biocompatibility and functionality have been verified following a systematic approach, from the in-vitro condition within glioblastomas multiform tumor neurospheres, the material has been tested in an in-vivo tumorigenicity assessment by xenograft transplantation into animal models. On one side, the magneto-responsive functionality enables a non-invasive in vivo imaging and enables the tracking of the brain tumor cell infiltration responsible of the disease recurrence. On the other side, the fluorescent functionality gives an excellent feedback on the biological environment dysregulation with microscopic resolution in biopsy sampled tissues. Most importantly for clinical applications, we demonstrate that fluoro-magnetic

	chrysotile nanotubes can spontaneously reach the brain tumor area after systemic intravenous injection by migrating across the blood brain barrier (BBB), preserving their functionalities, which can be exploited to map the brain cancer spread. Since the BBB is the main obstacle in tumor brain treatment research blocking the delivery of drugs to brain tissues, it represents the major drawback for the treatment of the diseases of the central nervous system. Therefore, our results strongly push forward the design and engineering of chrysotile-derived nanotools not only for diagnostic applications but to specifically achieve effective drug delivery across the BBB and to enhance the brain cancer treatment success probability. Besides the potential applicative impact of a new class of biocompatible fluoro-magnetic systems for clinical diagnosis technologies, our results provide a general strategy for the realization of unprecedented multifunctional materials for effective in-vivo multimodal theranostics of the brain cancer. The proposed approach is indeed not composition specific, and could in principle be extended to the use of a plethora of functional moieties such as drug delivery systems, labelling dyes, thermosensitive systems or reactive oxygen species sensors. We expect the newfound synthetic route to trigger intense research not just in the inorganic nanomaterials community, but also in the vast communities of supramolecular chemistry, fluorescence imaging microscopy, molecular biology and nanomedicine. We therefore believe that this work will be of interest to a broad audience of materials' scientists, bio-physicists, chemists, biologists and medical doctors. For these reasons, we hope that this manuscript might be found suitable for the general readership of Advanced Functional Materials. Sincerely, Angelo Monguzzi
Do you or any of your co-authors have a conflict of interest to declare?	No. The authors declare no conflict of interest.
Corresponding Author Secondary Information:	
Corresponding Author's Institution:	Universita degli Studi di Milano-Bicocca
Corresponding Author's Secondary Institution:	
First Author:	Angelo Monguzzi, Ph.D.
First Author Secondary Information:	
Order of Authors:	Angelo Monguzzi, Ph.D.
	Chiara Villa, PhD
	Marcello Campione, Associate Professor
	Beatriz Santiago-Gonzalez
	Francesco Alessandrini
	Silvia Erratico
	Ileana Zucca
	Maria Grazia Bruzzone
	Laura Forzenigo
	Paolo Malatesta
	Michele Mauri
	Sergio Brovelli
	Yvan Torrente
	Francesco Meinardi

	Elena Trombetta
Order of Authors Secondary Information:	
Abstract:	Fluoro-magnetic systems have been recognized as an emerging class of materials with great potential in the biomedical field. Here, we show how to fabricate fluoro-magnetic nanotubes that can serve as multimodal probes for the imaging and targeting of brain cancer. We use an ionic self-assembly strategy to functionalize the surface of synthetic chrysotile nanotubes with pH-sensitive fluorescent chromophores and ferromagnetic nanoparticles. The acquired magnetic properties permit their use as contrast agent for magnetic resonance imaging, and enable the tracking of tumor cell migration and infiltration responsible for metastatic growth and disease recurrence. Their organic component, changing its fluorescence attitude as function of local pH, targets the cancer distinctive acidity, and allows localizing and monitoring the tumor occurrence and progression by mapping the acidic spatial distribution within biopsy tissues. The fluoro-magnetic properties of nanotubes are preserved from the in vitro to the in vivo condition and that they show the ability to migrate across the blood brain barrier, thus spontaneously reaching the brain tumor after injection. The simplicity of the synthesis route of these geo-mimetic nanomaterials combined with their demonstrated affinity with the in vivo condition strongly highlight their potential for developing effective functional materials for multimodal theranostics of brain cancer.

Self-assembled pH-Sensitive Fluoro-Magnetic Nanotubes as Archetype System for Multimodal Imaging of Brain Cancer

Chiara Villa[a], *Marcello Campione*[b], *Beatriz Santiago-Gonzalez*[c], *Francesco Alessandrini*[d], *Silvia Erratico*[e], *Ileana Zucca*[f], *Maria Grazia Bruzzone*[g], *Laura Forzenigo*[h], *Paolo Malatesta*[d,i], *Michele Mauri*[c], *Elena Trombetta*[l], *Sergio Brovelli*[c], *Yvan Torrente*[a,e] , *Francesco Meinardi*[c] *and Angelo Monguzzi*[c]*.

[a]Stem Cell Laboratory, Department of Pathophysiology and Transplantation, Università degli Studi di Milano, Fondazione IRCCS Ca' Granda Ospedale Maggiore Policlinico, Centro Dino Ferrari, via F. Sforza 35, 20122 Milan, Italy.

[b]Dipartimento di Scienze dell'Ambiente e della Terra, Università degli Studi Milano Bicocca, Piazza della Scienza, 20125 Milano, Italy.

[c]Dipartimento di Scienza dei Materiali, Università degli Studi Milano Bicocca, via R. Cozzi 55, 20125 Milano, Italy.

[d]Dipartimento di Medicina Sperimentale (DiMES), Università di Genova, viale L.B. Alberti 2, 16132 Genova, Italy.

[e]NovaYstem Srl - Viale Piave 21, 20129 Milano, Italy.

[f]UO Direzione Scientifica, Fondazione I.R.C.C.S. Istituto Neurologico Carlo Besta, via Celoria 11, 20133 Milano, Italy.

[g]UO Neuroradiologia, Fondazione I.R.C.C.S. Istituto Neurologico Carlo Besta, via Celoria 11, 20133 Milano, Italy.

[h]Radiology Unit, Fondazione IRCCS Ca' Granda Ospedale Maggiore Policlinico, via F. Sforza 35, 20122 Milano, Italy.

[i]Ospedale Policlinico San Martino – IRCCS per l'Oncologia, Largo Rosanna Benzi 10, 16132 Genova, Italy.

[l] Flow Cytometry Service, Central Laboratory, Fondazione IRCCS Ca' Granda Ospedale Maggiore Policlinico, via F. Sforza 35, 20122 Milano, Italy

Corresponding Author
*Email: angelo.monguzzi@unimib.it

KEYWORDS
multifunctional probes – self-assembled nanomaterials - fluoro-magnetic nanotubes – cancer imaging – blood brain barrier

ABSTRACT

Fluoro-magnetic systems have been recognized as an emerging class of materials with great potential in the biomedical field. Here, we show how to fabricate fluoro-magnetic nanotubes that can serve as multimodal probes for the imaging and targeting of brain cancer. We use an ionic self-assembly strategy to functionalize the surface of synthetic chrysotile nanotubes with pH-sensitive fluorescent chromophores and ferromagnetic nanoparticles. The acquired magnetic properties permit their use as contrast agent for magnetic resonance imaging, and enable the tracking of tumor cell migration and infiltration responsible for metastatic growth and disease recurrence. Their organic component, changing its fluorescence attitude as function of local pH, targets the cancer distinctive acidity, and allows localizing and monitoring the tumor occurrence and progression by mapping the acidic spatial distribution within biopsy tissues. The fluoro-magnetic properties of nanotubes are preserved from the *in vitro* to the *in vivo* condition and that they show the ability to migrate across the blood brain barrier, thus spontaneously reaching the brain tumor after injection. The simplicity of the synthesis route of these geo-mimetic nanomaterials combined with their demonstrated affinity with the *in vivo* condition strongly highlight their potential for developing effective functional materials for multimodal theranostics of brain cancer.

1. Introduction

A very dynamic research area focuses on the design and synthesis of nanomaterials that simultaneously contain more than one functional component, so-called *multifunctional*, which are expected to have a significant impact on a wide range of applications. [1-5] Especially for *in-vivo* uses, the availability of multimodal sensing or multifunctional drug delivery/imaging materials can allow the combination of different diagnostic and/or therapeutic techniques in a single platform, thus leading to a potential reduction in side effects, risks, and costs, while increasing the benefits obtained from the synergy of different methods. [6-8] Recently, fluoro-magnetic particles have been recognized as emerging class with a huge potential. [9-13] Magnetic nanoparticles can be coupled to drug molecules, fluorescent compounds and various hydrophobic and hydrophilic coatings, opening up great prospects in both nano- and biotechnology by enabling the engineering of unique multimodal sensing/imaging targeted nanoscale devices. Therefore, much effort has been devoted to develop synthetic strategies for the fabrication of such materials, including heterostructure crystal growth,[14,15] co-encapsulation into organic/inorganic structures,[16] template-based synthesis via either chemical bonding or physical attachment,[17, 18] and co-assembling to form colloidal super-nanoparticles.[9]

In this work, we propose a step forward in this research by introducing the use of multi-functionalized geo-mimetic nanotubes as probes for pH-sensitive fluorescence imaging and magnetic resonance (MR) imaging of cancer tissues. We focused on a pH-reactive functionality because the changes in the acid–base balance of tissues is associated to many pathological states and, specifically, to the tumor environment. [19-21] The acidity of tumors is due to several factors including poor blood perfusion, low oxygen availability,[22] increased glucose metabolism and metabolic acid production and, moreover, the acidic extracellular milieu has been also demonstrated to favor tumor growth and invasion, playing a role in the aggressive metastatic development. [23, 24] Therefore, the pH fluctuation can be considered both as prognostic value and predictive for cancer treatment efficacy in order to develop more sensitive and faster diagnostic/therapeutic protocols. [25-27] However, although the monitoring of body fluids can give a precise indication of systemic acid–base imbalance, there is a serious lack of tools for mapping the pH spatial distribution in human tissues and patients with high resolution. Clinical applications require indeed not only accurate and precise non-invasive technologies, but also

quantitative imaging of biopsy material for improved differential diagnosis and monitoring of tumors invasion and metastasis formation. [5] This lack is especially evident in the neurosurgery and neurology medical areas, since the treatment of brain tumors, now often fatal in 1-2 years from the diagnosis, requires more efficient methodologies to identify the disease and understand its development in the very early stage. The occurrence of brain blood barrier (BBB) that makes difficult the delivery of probes and drugs to the brain is an additional particularly challenging issue for the development of specific imaging techniques, and poses extreme difficulties in finding effective treatments. [28] However, lethal malignant brain tumors such as the glioblastoma multiforme (GBM) are histologically characterized by pronounced hypercellularity, nuclear atypia, mitosis, necrosis of foci, and blood vessel morphological alterations that lead to a poorly developed BBB and increased vascular permeability. [29] In particular, in these cases the BBB is built on several pores with different sizes determined by trans-endothelial cell fenestrations, caveolae and vesiculo-vacuolar organelles, and inter-endothelial cell gaps between endothelial cells. The first ones present sizes ranging between 40 nm and 200 nm in diameter, while the inter-endothelial cell gaps are even larger, with diameters in the 100-3000 nm range. [30] Therefore, by taking in to account this porosity distribution available to accessing the brain, we aim at establishing a general design strategy for fabricating a multifunctional nanomaterial that provide information about the brain cancer evolution using both magnetic and optical diagnostic tools having a safe and functional access to the brain.

We use chrysotile nanotubes as fundamental building block because they are stable and non-toxic systems [31, 32] that, unlike similar and well known materials that would be used in bio-related applications such as carbon nanotubes, [33] they can be prepared by a rapid one-step hydrothermal synthesis in aqueous environment with controllable nanometric sizes (100-1000 nm) compatible with the cellular uptake and with the BBB porosity size in sick organisms, thus being suitable for administration by systemic intravenous infusion. It is worth pointing out that the possibility to control the nanotube size allows either to test the systemic intravenous administration or to choose alternative *in vivo* administration routes towards the central nervous system that would readily cross it (i.e. intranasal delivery). [34,35] Thanks to their charged surfaces, the chrysotile nanotubes have been functionalized through a multistep procedure with pH-sensitive fluorescent chromophores and magnetic

nanoparticles (MNP) by means of an ionic self-assembly strategy. The material biocompatibility and functionality have been tested following a systematic approach, from the *in-vitro* condition within tumor stem-like cells forming neurospheres to an *in-vivo* tumorigenicity assessment by xenograft transplantation into animal models. On one side, the magneto-responsive functionality enables a non-invasive *in-vivo* imaging and tracking of the tumor cells infiltration, responsible of the disease recurrence and of the tumor growth throughout the time. On the other side, the fluorescent dye gives a feedback on the biological environment dysregulation towards the acidic conditions mapping of the disease evolution in sampled tissues with microscopic resolution. In order to highlight their potential for clinical use, we demonstrate that fluoro-magnetic nanotubes systemically injected into an experimental model of glioma are indeed able to migrate across the BBB while maintaining their pH-sensitive fluorescence and magnetic properties. [36] Furthermore, the *in vivo* massive presence of systemically injected nanoprobes within the tumor suggests an effective tissue penetration, likely mediated by fenestrated tumor vessels. [37] The results obtained, together with the simplicity and generality of the synthetic route employed, demonstrate how functionalized geo-inspired materials can represent a versatile platform for the future development of multifunctional nanotools for effective *in-vivo* theranostics of brain cancers.

2. Synthesis and properties of fluoro-magnetic nanotubes.

Figure 1a is a schematic depiction of the fluoro-magnetic nanoprobes (from here called FluoroMags) synthesis protocol. The positive electrostatic potential of their surface is particularly prone for anchoring anionic species in aqueous environment following an ionic self-assembly scheme (ISA, Fig. 1a).[38] The ISA takes advantage of the Coulombic attraction between oppositely charged components, resulting in a simple bottom-up approach of wide applicability that enables for the fabrication of complex systems.[39, 40] The transmission electronic microscopy (TEM) imaging of the obtained material in Fig. 1b demonstrates the reliability of this method, which results in nanotubes with an inner diameter of 7 nm, an outer diameter of 50 nm, and length in the range between 200 and 1000 nm. The magnetic functionality is introduced through the

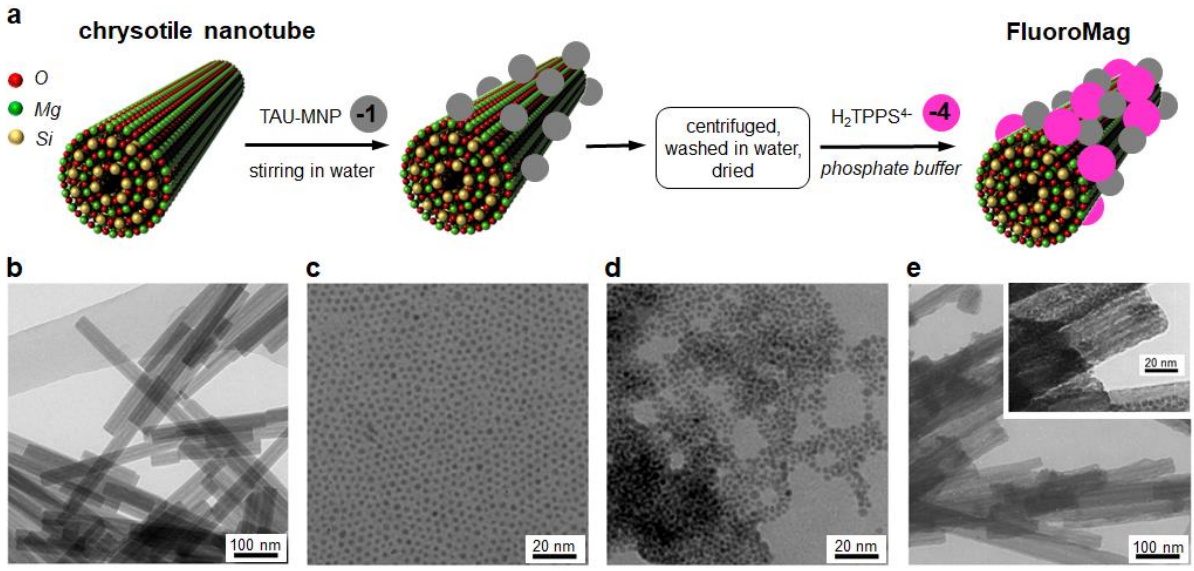

Figure 1. a) Chrysotile nanotubes were prepared in water and suspended in a phosphate buffer at pH=7.4. An equally buffered solution of [TAU^-]-capped magnetic nanoparticles (TAU-MNPs) was added under stirring. MNPs (grey dots) adsorb on the uncovered surface of the nanotubes thanks to the ionic self-assembly driven by the interaction between the positively charged nanotubes surface and the negatively charged [TAU^-] functionality. The obtained magnetic powder was then re-dispersed in a phosphate buffer solution, and the ionic self-assembly procedure was repeated by adding a H_2TPPS^{4-} fluorescent porphyrin solution (pink dots) to obtain the FluoroMags. b-e) Transmission electron microscopy (TEM) images of naked nanotubes (b), TAU-MNPs as synthesized (c) and after phase transfer in water (d), and FluoroMags (e). The inset of panel e is a magnification showing the MNPs (black dots) adsorbed on the nanotubes surface.

ionic interaction between nanotubes and tetramethyl ammonium 11-aminoundecanoate (TAU^-)-capped Fe_3O_4 nanoparticles (~7 nm, Fig. 1c and d, see Experimental Section). Thanks to the anionic functional groups $–COO^-$ of the capping ligands, the MNP nanoparticles are then attached onto the nanotubes surface. In the same way, the fluorescent functionality is then introduced by the addition of anionic tetra(4-sulfonatophenyl)porphyrin (H_2TPPS^{4-}), which saturates the positively charged nanotubes surface partially covered by MNPs, thus obtaining the final composition of the FluoroMags (Fig. 1e). Surface functionalization of chrysotile nanotubes has been furtherer confirmed by ζ-potential measurements on diluted colloidal aqueous dispersions (supporting Fig. S1). The pH-sensitiveness of the obtained material is given by the peculiar photophysical properties of H_2TPPS^{4-}. By increasing the acidity of the environment, the intramolecular dipole moments developed upon protonation triggers the assembly of porphyrins as head-to-tail aggregates, resulting in a quick reduction of the isolated-chromophore red fluorescence. This mechanism is strongly catalyzed by the nanotubes surfaces, which enhances the response of FluoroMags to the pH changes and, importantly, it is full reversible.[31, 41]

The dual functionalization of nanotubes has been confirmed by side-by-side optical spectroscopy and magnetic resonance (MR) experiments. Figures 2a and 2b show the optical properties of a FluoroMags dispersion in a phosphate buffer at pH=7.4. The UV-Vis absorption spectrum (Fig. 2a, green line) is identical to that one of H_2TPPS^{4-} in solution (blue line), except for the background signal due the partial scattering of the incident light. The main absorption band (*B*-band) is centered at 410 nm, accompanied by a series of less intense peaks (*Q*-band) at 516 nm, 550 nm, 581, and 635 nm.[42, 43] This latter optical transition is the responsible of the FluoroMags photoluminescence (PL) reported in Fig. 2b. The emission has a broad profile peaked at 648 nm with a secondary peak at 708 nm, and it decays as single exponential function with a characteristic lifetime of ~10 ns typical of fluorescent compounds (Fig. 2c). This indicates that the porphyrins preserve their PL properties even upon adsorption on the nanotubes surface without any evidence of aggregation and/or emission quenching, which would result in a multi-exponential decay of the PL signal.[44] These findings demonstrate the validity of the ISA as non-aggressive assembly method, which results in functionalized nanotubes that works as efficient fluorophores. Importantly for applications, the material has a very good stability, showing unchanged PL properties after one month of storage in air (Fig. 2b, crosses). The FluoroMags pH sensitiveness has been monitored by progressively adding hydrochloric acid (HCl) to the dispersion (Fig. 2b). As expected, the PL red shift (inset) and switches off upon increasing the acidity because of the aggregation induced emission quenching mechanism previously reported,[41] as further demonstrated by the faster signal decay observed at low pH values (Fig. 2c). After confirmation of their fluorescence properties, we proceeded to evaluate the magnetic relaxivity constant r_2 of FluoroMags. Fig. 2d shows the measurements of the transverse magnetic relaxation rate R_2 as a function of the nanotubes concentration in an aqueous suspension (see Experimental Section). R_2 shows a linear dependency which, importantly, indicates that FluoroMags are stable systems that does not experience any aggregation or splitting of the nanoassembly that would change qualitatively the interaction with water and therefore affect R_2.[45] From the slope of the linear regression of the experimental date we were able to estimate a relaxivity of r_2= 402 s^{-1} $(g/l)^{-1}$. Using the same approach (see Supporting Fig. S2) we estimated also the longitudinal relaxivity constant r_1 = 48 s^{-1} $(g/l)^{-1}$, resulting in a r_2/r_1 ratio of about 8.4. This high value indicates that FluoroMags are indeed suitable as negative contrast agents for MRI.[45]

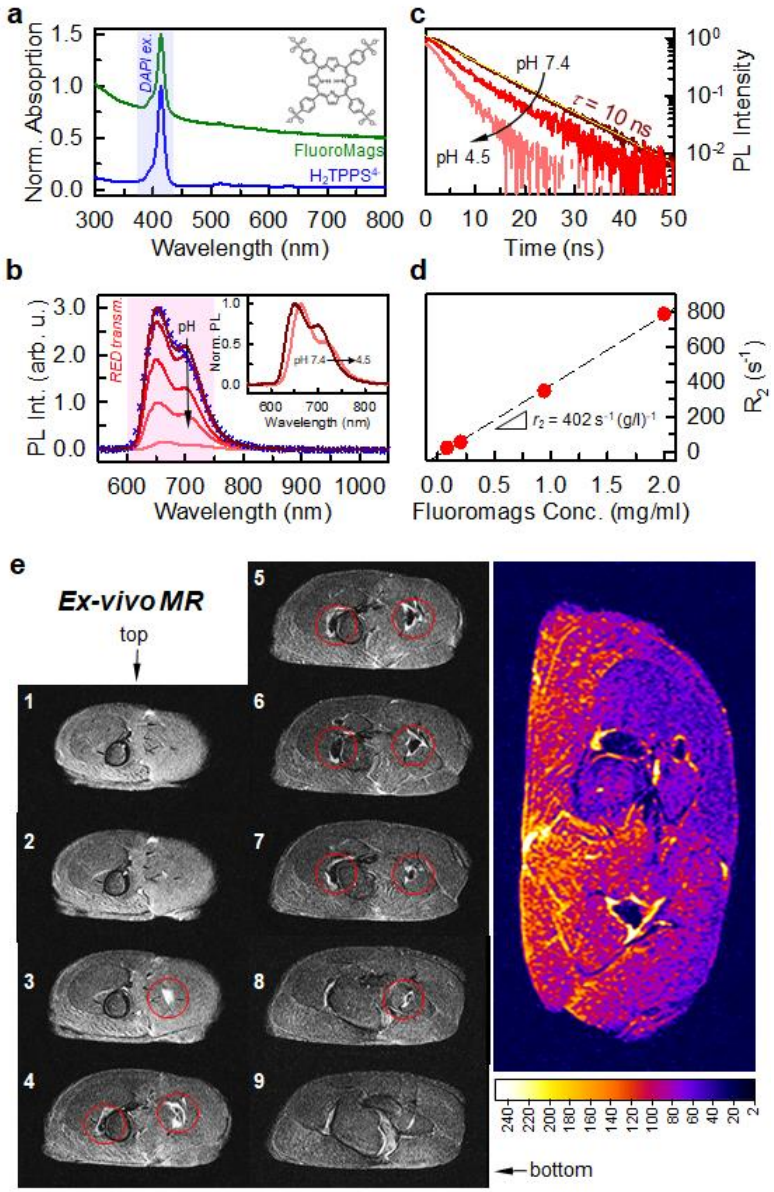

Figure 2. a) Normalized absorption spectrum of H_2TPPS^{4-} porphyrin solution and a FluoroMags dispersion in aqueous phosphate buffer at pH = 7.4. The inset depicts the molecular structure of H_2TPPS^{4-}. The shaded vertical stripe indicates the excitation range of the DAPI standard dye for nuclear cellular staining. b) Photoluminescence (PL) profile a FluoroMag suspension under 405 nm pulsed laser excitation a function of the pH which has been decreased from 7.4 (dark red line) to 6.5, 6.0, 5.5 and 4.5 (pink line), respectively. In the neutral condition, the FluoroMags show the same PL shape even after one month of storage in air (blue crosses). The shaded stripe marks the transmission band in the red spectrum of a commercial confocal microscope for fluorescent bio-imaging. The inset reports the normalized PL spectrum of FluoroMags under 405 excitation recorded in aqueous dispersion at pH 7.4 and 4.5, respectively. c) Time-resolved PL decay dynamics at 648 nm at pH = 7.4 (circles). The signal decays as a single exponential function with a characteristic time of 10 ns (yellow line). Upon increasing the solution acidity to pH = 4.5 the FluoroMags PL lifetime is significantly shortened and show a multi-exponential behavior (squares). d) Measurement of the FluoroMags magnetic relaxation rate R_2 as a function of the concentration in aqueous suspension. e) Two areas of hypo-intense signals were seen by *ex-vivo* MR imaging after injection of 10^6 FluoroMag-labeled NIH/3T3 fibroblast cells into a chicken breast (red circles). The color panel is a magnification of image 6, with a scale bar indicating the intensity of the magnetic response of the different areas of the sample.

Remarkably, r_2/r_1 is in good agreement with the magnetic responsiveness of superparamagnetic iron nanoparticles which are significantly larger than the MNPs used here.[46] This further demonstrate that MNPs are not dispersed individually in the solution, but rather properly carried on the surface of chrysotile nanotubes where cooperatively contribute to the responsiveness of the material to the external magnetic field. FluoroMags have been then used to label an immortalized fibroblast cell line (NIH/3T3) which has been injected into a chicken breast for an *ex-vivo* MR imaging experiment. Fig. 2e shows that FluoroMags works as hypo-intense MR contrast agent (red circles in b/w images and blue area in the color image), definitely proving the effectiveness of the dual-functionalization of nanotubes described above to obtain an optically- active and magneto-responsive nanomaterial. It is worth pointing out that the FluoroMags optical properties match the technical specifications of commercially available fluorescence microscopes (shaded stripes in Figs. 2a and 2b). The excitation band in the UV-Vis range is the one commonly exploited for the DAPI dye, used for nuclear cellular imaging,[45] while the photoluminescence spectrum corresponds to the emission range of several commercial red fluorophores, i.e. the Texas Red.[48] Therefore, the FluoroMags can be employed "as is" with the equipment commonly available for research use and biomedical analyses by MR and optical fluorescence microscopy.

3. In-vitro experiments.

With the aim to show the FluoroMags translational potential and to verify their stability in biological media, we performed a series of *in-vitro* viability assessments and imaging experiments on NIH/3T3 fibroblasts. We used the 3-(4,5-dimethylthiazol-2-yl)-2,5-diphenyltetrazolium bromide essay (MTT) to evaluate the nanoprobes cytotoxicity by monitoring the cellular proliferation.[49] Figure 3a shows the MTT results obtained on cells labeled with increasing FluoroMags concentrations after 24 hours of incubation in controlled atmosphere at 37°C (5% CO_2). Overall, the data shows no evidence of cytotoxicity. In particular, the staining with 25 μg cm^{-2} FluoroMags solution does not affect the cellular proliferation, which remains strictly comparable to unlabelled cells used as control experiment (CTR). The immunofluorescence test confirms this result. Fig. 3b reports representative bright field and RGB (red-green-blue) images of the NIH/3T3 cells stained with red-emitting FluoroMags (red), green-emitting calcein-AM (green), and blue-emitting Hoechst (blue). Calcein-AM is a specific marker for the

cytoplasm of living cells, which enables to monitor the effect of a labelling on the cellular vitality, while Hoechst is a nucleus counterstaining.[50] The images confirm the uptake of FluoroMags, which diffuse into cells via non-specific pathways because of the lack of any targeting functionality. The good overlap of RGB channels demonstrates that the red staining does not stress significantly the cellular viability, despite the nanotubes shows a

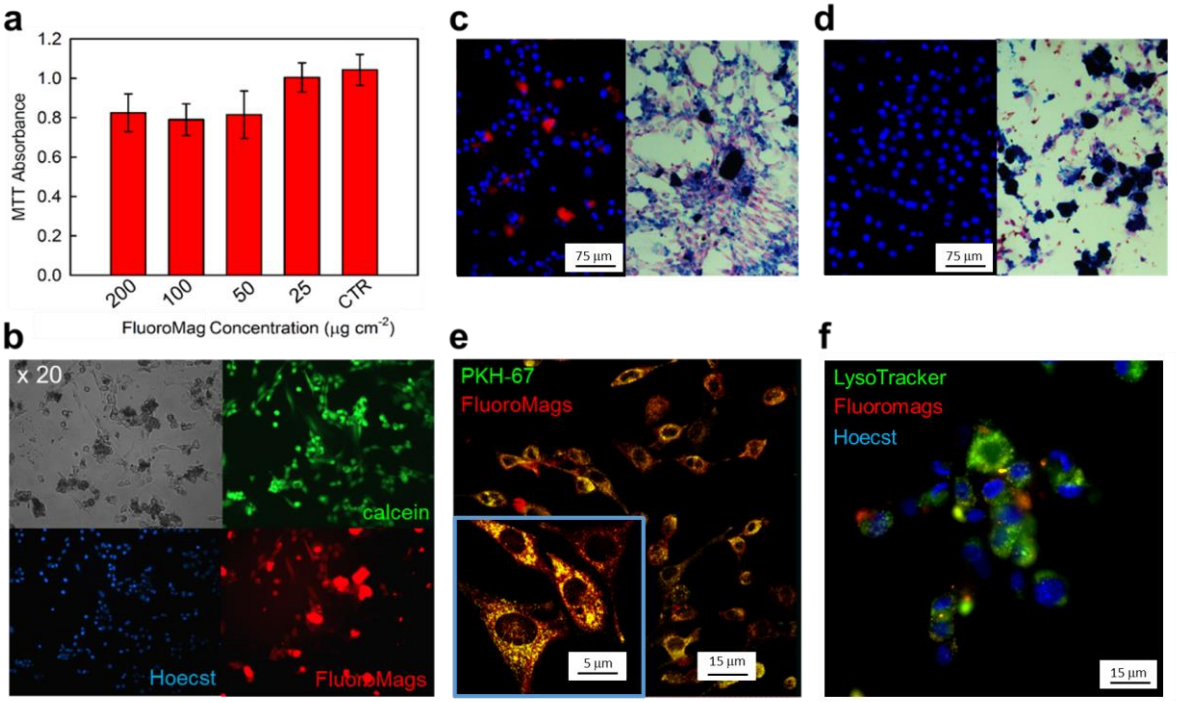

Figure 3. a) MTT test results on NIH/3T3 cells after 24 hours labelled with a decreasing FluoroMags concentration. b) Image of living cell labelled with Hoechst (blue nuclei), calcein-AM (green cytoplasm) and FluoroMags (25 μg cm^{-2}, red cytoplasm and aggregates). c, d), The response of the stain to the environmental pH has been observed by recording the far-field fluorescence imaging together with the Hoechst nuclei counterstaining (left panels) in neutral and acidic environment, respectively. The histology (right panels) confirms positive Prussian blue labeled NIH/3T3 cells in both conditions demonstrating the stable inclusion of FluoroMags, selectively marked by the blue dye. e) Confocal fluorescence images of NIH/3T3 cells a t pH=7.4 stained with PKH-67 (green signal) and FluoroMags (red signal) under 410 nm laser excitation. f) Confocal fluorescence image of lysosome staining by LysoTracker Green DND-26 (green signal) in FluoroMags (red signal) labeled human glioblastoma (GBM) derived adherent cells. Nuclei were counterstained by Hoechst (blue signal).

tendency to aggregate. In order to check the FluoroMags uptake stability and fluorescence responsiveness in an acidic environment mimicking the tumor, we added to the cells culture medium a titrated HCl solution. The left panels of Fig. 3c and d report the far-field fluorescence image of cells labelled with FluoroMags (red) and Hoechst (blue). As a proof of concept experiment, from the initial value of 7.4, the pH has been reduced to 4, observing a corresponding decrease of the FluoroMags fluorescence that prevents their visualization. Notably, the quick answer to environment acidity

dysregulation demonstrates that internalized FluoroMags are not trapped in subcellular structures that hinder interaction with their chemical surroundings.[51] Indeed, in such a case the material would be insensitive to any external pH changes, in contrast with the experimental evidences. In order to visualize the FluoroMag retention at reduced pH, the cells have been subsequently stained with the Prussian blue dye, which is a selective marker for ferromagnetic particles.[52] In such a way, the FluoroMags can be visualized in the bright field mode (right panels) thanks to the blue staining of the MNPs on their surfaces. It should be noted that this forced rapid drop of pH constitutes an extremely harsh environment for the *in-vitro* cell viability, as suggested by the loss of volume and shrinkage of fibroblasts. However, they exhibit a stable internalization of FluoroMags even in this condition of severe insult, except for an evident nanotube aggregation likely due to the morphological changes and nuclear condensation signatures of stressed cells.[53, 54] The FluoroMags staining ability in pH-balanced conditions is confirmed by the high-resolution fluorescence imaging of NIH/3T3 cells reported in Fig. 3e, where the cellular membrane has been labelled with the specific marker PHK-67 (green). The internalized nanotubes display a red fluorescence diffused in cytoplasm without any evidence of aggregates. It is worth pointing out that after cell entrance FluoroMags can undergo different intracellular fates, among which they may be delivered towards the endosomal/lysosomal systems, and get accumulated.[55] Given that lysosomes are dynamic acidic organelles (pH 5-5.5), FluoroMags uptake within them may result in an unspecific decreased fluorescent signal, independently from the tumor acidic level, thus representing a big hurdle for their use for affordable for brain cancer imaging. In order to shed light on the fate of internalized nanoprobes, we performed lysosomal staining of FluoroMags labeled human glioblastoma (GBM) derived adherent cells throughout the LysoTracker Green DND-26 dye. Representative confocal microscopy images of stained cells showed the distinct fluorescent signals of LysoTracker (green) and FluoroMags (red) with very low overlap, indicating that most nanofibers escaped from vesicular compartments to the cytoplasm, where they can freely react to any acidity change of the intracellular environment and therefore act as effective pH sensors in brain tissues. The pH sensitive fluorescence of FluoroMags labeled NIH/3T3, has been further confirmed by Fluorescence-activated cell sorting (FACS) flow cytometry analysis (Figure S2), which show a decrease of the intensity of the fluorescence emitted from the internalized probes at increased acidity conditions.

In order to approach the real condition of the disease in living tissues, we made a step forward by testing the FluoroMags in a carcinogenic model system *in vitro*. Figure 4 reports the imaging cultured neurospheres derived from human GBM (GBM-NS, Fig. S3) and labelled with FluoroMags. GBM have been known to include terminally differentiated cells, progenitors, and stem-like cells. The latter are capable of giving rise to cells expressing markers of primary neurons and glial cells such as astrocytes and oligodendrocytes, as well as being able to self-renewal and aggregate in suspension into spheres.[56]

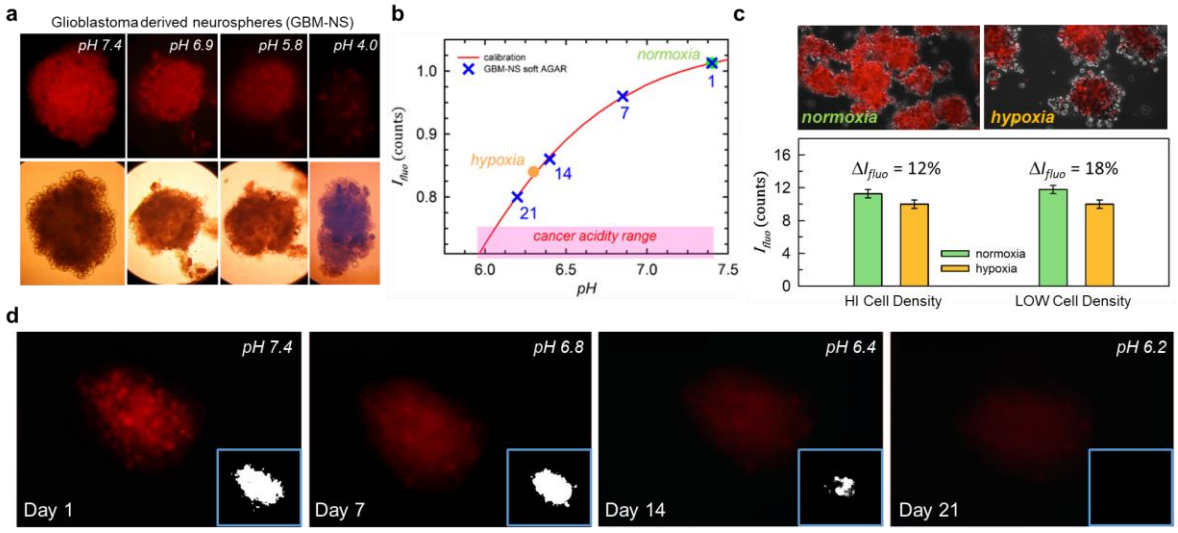

Figure 4. a) Fluorescence and optical images of FluoroMags stained GMB-NSs recorded in a neutral to acidic environment after addition of HCl. b) Calibration curve of FluoroMags pH-sensitiveness. The solid line indicate the intensity of red fluorescence as a function of the environment acidity in the "cancer sensitive" pH range between 6.0 and 7.5. c) Fluorescence imaging of two samples of GBM-NSs in standard oxygenation condition (*normoxia*) and hypo-oxygenated condition (*hypoxia*). On average, the fluorescence intensity I_{fluo} decrease by a factor 16%, which allows for estimating a pH of 6.4 for the simulated hypoxic condition of cancer (green and orange dots in b). d) Fluorescence imaging of a GBM-NS formed within soft-AGAR in an anchorage independent fashion and reproducing the tumor formation as a function of time. The insets are high contrast black and white images of tumorigenic GBM-NSs obtained applying an intensity threshold filter of 20% on the red luminescence signal. The estimation of the fluorescence signal reduction enables to monitor the system pH evolution at each time point of the tumor formation (blue crosses in c).

Therefore, stem-like cells isolated from freshly resected human cancers have been used to grow *in-vitro* tumor models as GBM-NS. As showed in Fig. 4, in a neutral condition, we can image the system thanks to the FluoroMags fluorescence, and again we observe the quick answer to the pH lowering down to 4 upon HCl addition. A precise calibration curve for the FluoroMags sensitivity to pH changes has been obtained by increasing the material in acidic environment until a pH=2.0 has been reached (Fig. S4). However, in the perspective of a translational research we have to consider that the *in-vivo* local acidity of tumors is not increased to this extent, with pH values that are assessed in the range between 6.0 and

7.0 even into bulk tumor environments.[37] Notably, referring to the calibration curve for the intensity of the FluoroMag fluorescence I_{fluo} vs pH reported in Fig. 4b, the lowering of the pH to an average value of 6.5 will induce a I_{fluo} decrease of ~15%, a net change that should enable the pH-distribution mapping. Therefore, we settled an *in-vitro* tumorigenic assessment for a better reproduction of the real cancer environment in order to demonstrate the responsiveness of our probe in this pH analysis range. A factor strongly associated with malignancy and able to drive a tumor glycolytic shift towards acidosis is the chronic lack of oxygen arising in the tumor tissue.[57] This is mostly due to the abnormal and poorly functional vasculature of solid tumors, which does not supply sufficient oxygen to support growing tumor mass. The inadequate blood supply produces hypoxic conditions and a partial use of glycolysis that turns out in the cytosol acidification, high levels of protons and lactic acid, and eventually in acidic tumor extracellular environment. In particular, while levels of oxygen vary within brain tumors, hypoxic foci have been also associated with resistance to radiation and chemotherapies.[58, 59] Since most cells in tumors are exposed to oxygen tensions lower than 10 mmHg equivalent to <1.3% O_2 in vitro,[60] we simulated the disease condition by performing two different experiments. First, we compared I_{fluo} of stained GBM-NSs kept in standard oxygenation condition, *normoxia* (20% O_2*)*, with that one kept in a hypo-oxygenated condition, *hypoxia* (1% O_2). Fig. 4c reports explicative images of bright-red normoxic (left panel) and darker hypoxic (right panel) GBM-NSs. The experiment has been repeated two times by varying the *in-vitro* cell density in order to evaluate the FluoroMags sensitiveness independently from the number of cells. GBM-derived single cells suspensions were cultured at low (5×10^3 cells cm^{-2}) and high (50×10^3 cells cm^{-2}) concentration in serum lacking media containing growth factors to induce GBM-NS formation. The neurosphere generation occurred within the first week of culture. After 15 days on incubation in hypoxic atmosphere we observe an average variation ΔI_{fluo}= 16% (Fig.4c, low panel). Thus, we can affirm that hypoxic GBM-NSs, which specifically mimic a real tumor, are shifted from the neutral condition (green dot in Fig. 4b) to an acidic condition at pH = 6.35 (orange dot), in agreement with the literature data on similar situations. [61] These findings suggest that FluoroMags can be used to check the disease evolution by monitoring the tissues acidity, as further demonstrated by the second experiment. Forming GBM-NSs into a semi-solid gel, such as low concentrate agarose (soft-AGAR), is a common clonogenic/tumorigenicity assay that allows for an anchorage independent growth

of tumorigenic colonies from GBM isolated stem-like cells. In this condition, only highly proliferative subcloned cancer cells display a rapid growth, because of *in-vitro* carcinogenesis and *in-vivo* tumorigenic features of the colony. In other words, we fabricated an artificial self-assembled 3D tumor model aimed to reproduce precisely the cancer microenvironment in living tissues.[62] Fig. 4d reports the fluorescence imaging of a GBM-NS grown within the soft-AGAR matrix. As expected, the progressive evolution of the neurospheres initially composed of healthy cells (day 1) towards a natural tumor environment recapitulation (day 21) is accompanied by a pH reduction, as indicated by the net decrease of I_{fluo} that can be followed even by naked eyes. Importantly, for diagnostic and research applications the acidity change can be visualized in high-contrast mode by a simple post-processing of the acquired fluorescence images. The insets of Fig. 4d show the imaging of GBM-NSs obtained applying a threshold intensity digital filter. This procedure should allow for i) obtaining a precise black and white mapping of the healthy/sick cells and tissues, and ii) precisely monitoring the pH level. As indicated by the blue crosses in Fig. 4b, after 21 days of culture the tumorigenic GBM-NSs display a I_{fluo} reduction of ~20%, which corresponds to a pH decrease down to ~6.2, in agreement with the literature data.

4. In-vivo experiments.

Once assessed their features as multifunctional probes by *in-vitro* an *ex-vivo* tests, we performed two *in-vivo* experiments in order to demonstrate the potential of FluoroMags for parental use. In the first assay, labelled GBM-NSs give rise to brain tumor by orthotopic injection in nude mice, i. e. an immunodeficient mouse model. As depicted in Figure 5a, b freshly grown GBM-NSs labeled with FluoroMags were injected in the right hemispheres of the brain to seed the growth of a bulk tumor. A set of three animals has been treated and imaged by MR immediately after the xenotransplantation (time point zero, T0), and after 90 days (time point 1, T1) in order to respectively localize the injected labelled neurospheres and verify the appearance of a bulk tumor. The *in-vivo* MR imaging has been followed by mouse euthanasia through cervical dislocation for brain retrieval aimed at optimizing the experimental setup and, successively, at detecting the FluoroMags fluorescence signal within the host tissue. Fig. 5b is the MR imaging of the brain at T0. Thanks to the magnetic functionality of FluoroMags, GBM-NSs

can be easily visualized MR and, specifically, they have been found in the region between the slices II and III of the sampled tissue, in a brain region of ~ 600 μm thickness. In order to set the correct experimental parameters and to verify the inoculation, we performed a series of imaging experiments on the brain of a control mouse at T0. MR imaging data and the haematoxylin/eosin immunohistochemistry staining allows for the localization of the injected material (data not shown) employed for the immunohistochemistry analysis (Fig. 5c, white circle).

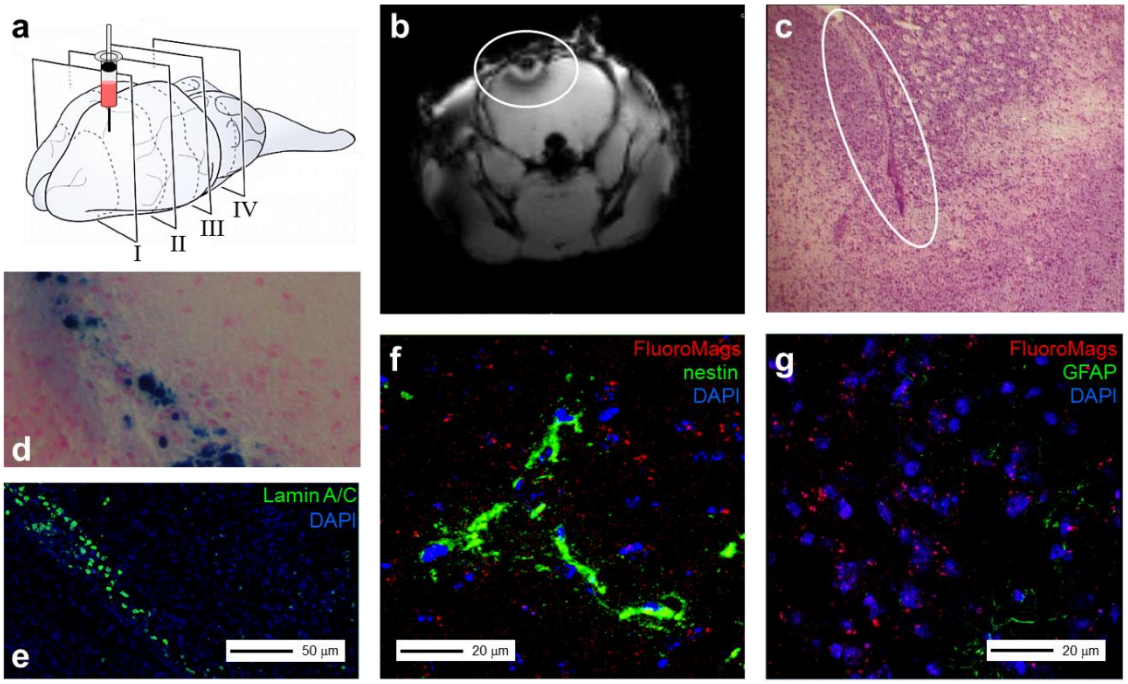

Figure 5. a) Sketch of the mouse brain showing the spot region where FluoroMag stained GMB-NSs have been injected. b) In-vivo MR imaging of the brain section between zone II and III, where the GBM-NSs have been localized thank to high contrast effect of FluoroMags on a T2*-weighted image (white circle). c) H&E immunohistochemistry of the brain slice outlining the injection area (white circle). d) Prussian Blue immunohistochemistry of the brain slice, and (e) with fluorescent dyes Lamin A/C (green, human cell nuclei) and DAPI (blue, cell nuclei). f, g) Fluorescence imaging of stained mouse brain slices containing FluoroMag stained GBM derived cells (red). The detection of the human nestin (f) and GFAP (g) expression proves respectively the presence of GBM-derived cancer neural progenitors and the absence of differentiated cancer cells immediately after inoculation, respectively.

T0 brain sections were stained with Prussian blue to visualize the presence of magnetic particles and with Lamina A/C, a specific luminescent green dye that that marks the nucleus of human cells.[63] The good overlap of optical and fluorescence images reported in Fig. 5d and 5e proofs the effective uptake of FluoroMags by GBM-NSs, and confirms that these latter have been properly included in the host organism. This is a crucial point, because it is pivotal that a multifunctional probe maintains its structural stability during the transfer procedure *in-vivo*. The lack of cancer in the host at T0 has been further

confirmed by an additional test. Fig. 5f and g report the fluorescence imaging of brain tissue stained with nestin and Glial Fibrillary Acidic Protein (GFAP), respectively.[64-67] Since these dyes are specific for undifferentiated human stem cells (nestin) and glial tumoral cells (GFAP), they allow either for visualizing normal undifferentiated stem-like cells, when the tumor is not yet formed, or differentiated cancer cells, when the disease has already induced a tumor glial expression (Fig. S5). While the red emission from FluoroMags is visible in both samples as expected in healthy tissues,

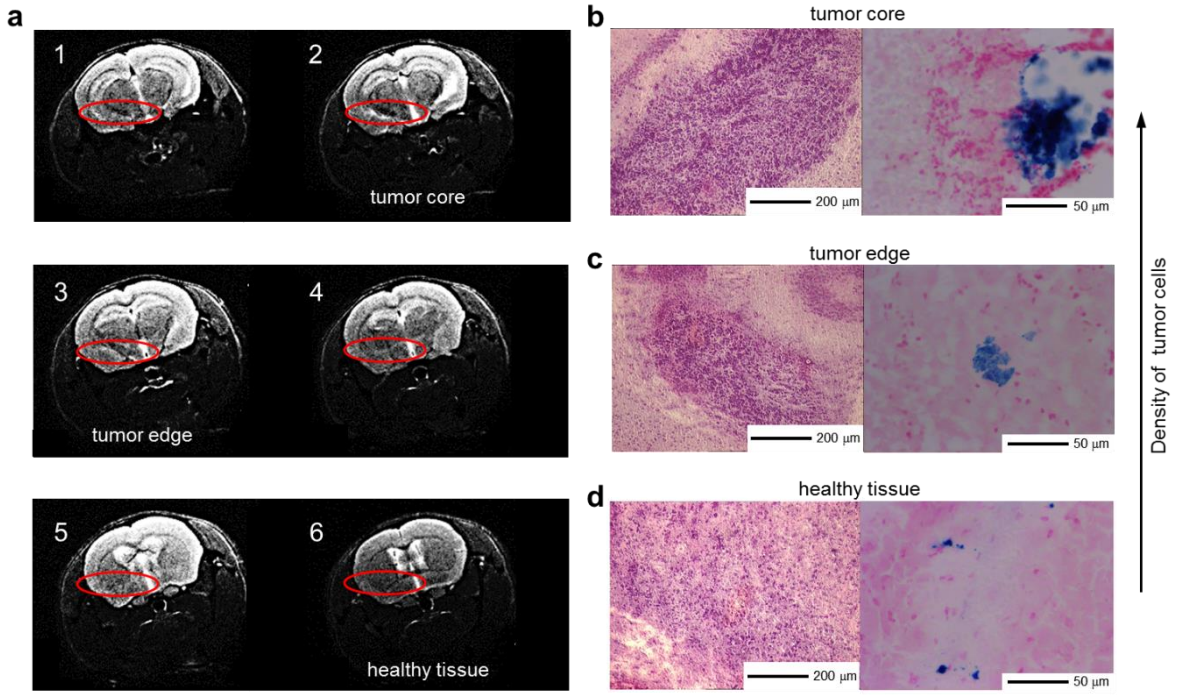

Figure 6. a) Sequential MRI slices (T2-weighted images, 1 caudal, 6 rostral) of the mouse brain after 90 days of GBM-NS transplantation, from the top of the head (1) to the deeper part close to the cerebellum (6). The red circle indicates the GBM-NS localization. Thanks to FluoroMags we are able to localize the core (2), peripheral part of the tumor tissue (tumor edge, 3), and to distinguish a healthy not affected tissue part (6). b-d) H&E immunohistochemistry of the tumor core (b), tumor edge (c) and the healthy not affected tissue (d). Accordingly, the intense staining with Prussian blue (right panels) show the higher density of tumor cells in the core of the tumor tissue in respect to the edge and the healthy zone.

only the nestin-stained sample shows a green luminescence, demonstrating the absence of tumor mass in the murine host brain at T0.

At T1, the precise spatial localization of the grown tumor has been performed by a sequential brain MR imaging, from the surface to the deeper part of the organ towards the cerebellar structures (Fig. 6a, from **1** to **6**). We distinguish three regions of interest. The most intense MR contrast (**2**) indicate the core of the tumor tissue derived from the inoculated GMB-NSs. Conversely, in the peripheral part of the tumor where a low amount of sick cells is present, the MR contrast fades away (**3**), resulting in images very

similar to that one recorded in the deeper, and healthy part of the brain (**6**), where almost none GBM-NSs is found. The immunohistochemistry images confirm this view (Fig. 6b-d), and interesting findings can been pointed out from the fluorescence imaging series reported in Fig. 7. Remarkably, in the core zone we can easily observe the GFAP green fluorescence, demonstrating the evolution of the stem-like GMB-NSs into fully expressed tumor glial cells, while the red fluorescence has completely disappeared in response to the tumor-induced acidity of the tissue (panel

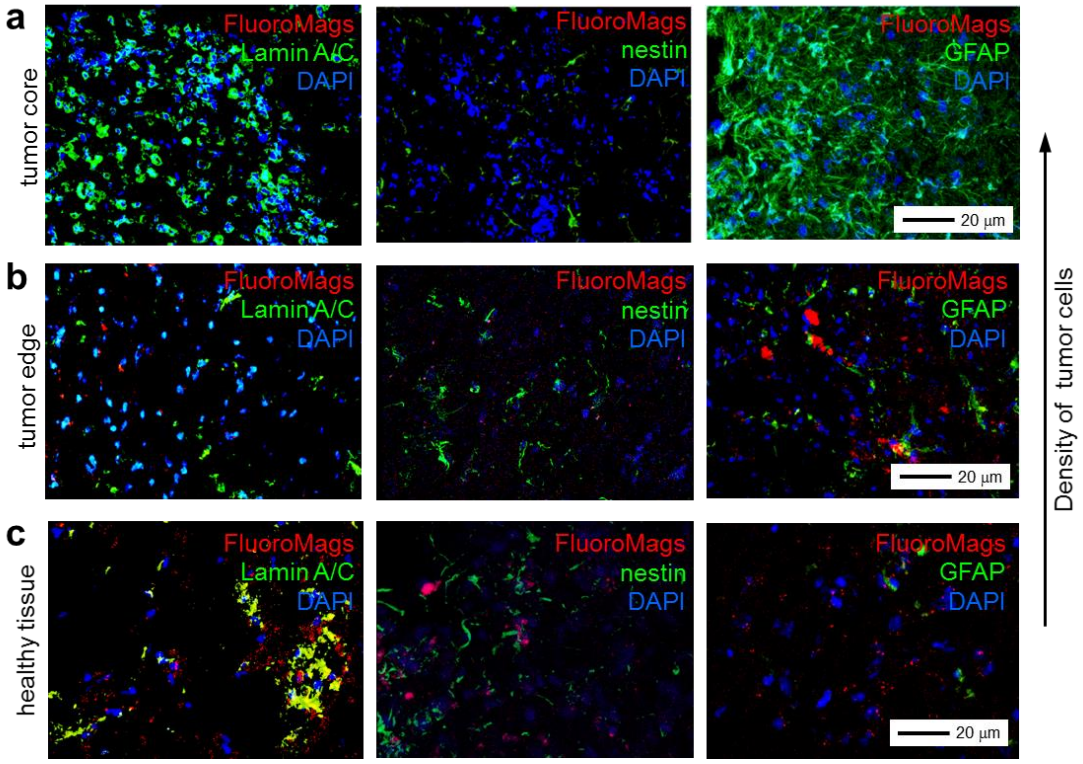

Figure 7. Immunofluorescence staining of brain tissue slice, from the tumor core (a), the tumor edge (b) and the healthy tissue (c). To confirm the presence of human cells the first slab has been stained with Lamin A/C. In addition, to enable the visualization of progenitor cancer cells we used nestin, while GFAP has been employed to image tumor glial human cells. Only in the tumor edge section and in the health not affected tissue section, we can observe the red luminescence from FluoroMags, while in the strongly acidic environment of the tumor core the red signal is completely suppressed.

a). Conversely, looking in the tumor peripheral part, were oxygenation is better thanks to the blood vessels of the host and therefore possess an almost neutral pH level, the FluoroMags emission is still visible (panel b). Similarly, in the healthy tissue the red fluorescent, isolated single cells are visible, together with the bright nestin staining (panel c). These results are fully consistent with the observed tumor distribution and its metabolic behavior that produce a hypoxic condition, and demonstrate that i) FluoroMags have been effectively included in GBM-NSs, ii) they keep their fluoro-magnetic properties

upon *in-vivo* transplantation and iii) their pH sensitiveness can be used to map the disease evolution and spread within biopsy sample tissues.

With the second in vivo experiment, we demonstrate that FluoroMags can cross the BBB of glioma tumor after intravenous systemic injection, which is a crucial feature for the use any nanotool aimed to reach the brain environment in living organisms for both drug delivery and diagnostic purposes. The main objective of this experiment is to explore the BBB penetration ability of FluoroMags. A group of four Ds-Red positive glioma animal models were systemically injected with 500 μg of FluoroMags dispersed in PBS, while a group of five Ds-Red positive glioma model was treated with pure PBS as control (Fig. S6). [36, 68] After euthanasia, FluoroMags has been localized within the brain through by H&E immunohistochemistry. As showed in Fig. 8a, the core of the Ds-red glioma tumor shows intense Prussian blue staining in close proximity tumor blood vessels (white circles). Only nanotubes injected animals shows positive Prussian blue results and the FluoroMags red emission in the brain with high distribution in tumor areas, thus indicating that the nanotubes can penetrate the BBB and reach the brain. With the aim to demonstrate that pH-sensitive behavior is preserved after systemic injection and can be exploited for optical tumor mapping, we analyzed the PL properties of brain delivered FluoroMags by confocal time resolved spectroscopy. Fig. 8b show the fluorescence imaging of a brain tissue sample were the signal of DsRed is shown (green, see Methods). This latter is a fluorescent reporter expressed by tumor cells that allows for the direct visualization of the edge (dashed line) between the tumor (green area) and the healthy area and the healthy area, which conversely, remains dark except for the bright red emission from FluoroMags. Weakly fluorescent nanotubes internalized in the tumor has been visualized with a blue pseudocolor to enable a better comparison of the data recorded on the PL properties reported in Fig. 8c. Under pulsed excitation at 405 nm the PL shape shows a slight red shift that suggests the effective environmental acidity increment by moving from the healthy to the tumor tissue. The time resolved analysis points out significant differences that further support this picture. According to the neutral pH level, the PL signal at 645 nm in the healthy tissue decays as single exponential (red solid line) as previously showed in Fig. 2c. Conversely, the PL decay within the tumor is strictly non-exponential (blue solid line), thus indicating the occurrence of aggregation induced quenching of the emitting chromophores on the FluoroMags surfaces in response to the lower pH value/higher local

acidity of the cancer environment. These findings unambiguously demonstrate that the pH-sensitive and magnetic functionality of FluoroMags are fully preserved after 7 days from the systemic injection and, remarkably, after passing the BBB thus reaching the brain tumor than would be imaged/treated. Of note, we found that FluoroMags are mainly located around vessels within and in close proximity of the brain tumor, suggesting that the peculiar tumor vessel fenestrated structures may exert dimensional tumor selectivity towards our nanoprobes. Further studies are still ongoing in order to shed light on this point.

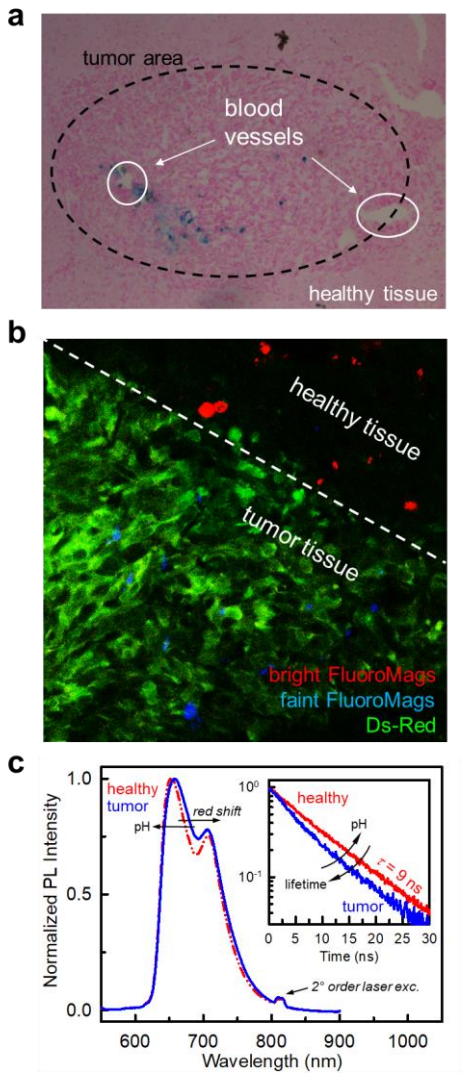

Figure 8. a) H&E immunohistochemistry of healthy edge (outside dot lane) and core (inside dot lane) Ds-red glioma tumor showed intense Prussian blue staining around tumor blood vessels (white circle). b) Immunofluorescence staining of brain tissue slice showed FluoroMags in edge healthy (NF healthy in red) and core tumor (NF tumor in blue pseudocolor). Tumor cells are visualized as green pseudocolor positive by the luciferase staining (see Methods). c) Confocal PL and time resolved PL (inset) of FluoroMags internalized in healthy (red) and tumor tissue (blue) respectively, under pulsed excitation at 405 nm.

Conclusions

In summary, we demonstrated how to fabricate a fluoro-magnetic probe that can be used for multimodal imaging of brain cancer through a multiple functionalization of inorganic chrysotile nanotubes, which have been upgraded by adding both a ferromagnetic and a pH-sensitive fluorescence functionality. Their biocompatibility, stability, responsiveness and efficiency as a contrast agent for magnetic and optical fluorescence imaging have been tested in a series of crossed experiments, spanning from the cellular level to the *in-vivo* environment of an induced brain tumor in mice. The results obtained demonstrate that these nanotubes can be used to study the disease evolution and, simultaneously, the eventual beneficial effects of a treatment that would restore the natural pH neutral condition of a healthy living organism. The versatility of the functionalization strategy employed makes these biocompatible geo-mimetic nanomaterials particularly prone to be combined with a plethora of labelling, fluorescence, magnetic and drug-related functionalities, recommending them as a new paradigm for the design and development of multifunctional materials with a broad application in bio-imaging, diagnostics and nanomedicine. In particular, the obtained results suggest that the use of pH-sensitive and near-infrared emitting materials, matching one of the transparency windows of the biological tissue, together with a proper labelling functionality can lead to the fabrication of effective *in-vivo* specific multimodal probes. The realization of such a material could represent a crucial step forward for the oncological research, because the availability of real time monitor of the tumor growth dynamic in model living organisms can enable a more accurate prediction of the disease clinical behavior and of the fate of the tumor initiating cells that infiltrate healthy tissues determining metastasis, tumor escape and recurrence. Most importantly for clinical applications, we demonstrate that FluoroMags can reach the brain tumor through the BBB after systemic intravenous injection by preserving their functionalities, which can be exploited to map the disease spread. Since the BBB is the main obstacle in tumor brain treatment research blocking the delivery of drugs to brain tissues, it represents the major drawback for the treatment of the diseases of the central nervous system. Therefore, our results strongly push forward the design and engineering of chrysotile-derived nanotools not only for diagnostic applications but to achieve effective drug delivery across the BBB and to enhance the brain cancer treatment success probability.

Experimental Section

Synthesis of stoichiometric chrysotile nanotubes. Chrysotile NTs with average length 1000 nm were synthesized according to the modification of the synthesis method reported in literature.[67, 69] A hydrothermal synthesis reactor with a 100 cm^3 moveable polypropylene vessel, was used to carry out the hydrothermal reaction of Na_2SiO_3 and $MgCl_2$ in an aqueous NaOH (0.4 M) solution at 250 °C, on the saturated vapor pressure curve (39 atm) and with a run duration of 24 h. The precipitate removed from the solution was repeatedly washed with deionized water before being dried for 3h at 110 °C.

Synthesis of Fe_3O_4 MNPs. Oleic acid-capped MNPs were synthesized in accordance to Sun and Zeng.[69] A ligand exchange protocol was applied to obtain hydrophilic MNPs with anionic functional groups as capping agents: A dispersion of MNPs in *n*-hexane (ca. 20 mg ml^{-1}) was added to a suspension of tetramethyl ammonium 11-aminoundecanoate (TAU^-) in dichlomethane (20 mg ml^{-1}). After vigorous stirring for 30 min, the particles were separated by using a magnet. The nanoparticles grown through this protocol has anionic functional groups (-COO^- of TAU) as capping agents.[70]

Synthesis of fluoro-magnetic nanotubes. Functionalized NTs were prepared in water in accordance with the ionic self-assembly procedure reported in De Luca *et al*.[31].In a typical reaction batch, 40 mg of chrysotile were suspended in 8 ml of 5 mM phosphate buffer at pH 7. An equally buffered solution of (TAU^-)-capped MNPs (2 mg ml^{-1}) was added slowly under vigorous stirring. Addition was stopped after ca. 10 ml, since the water started to assume a brownish color. At this point, the compound was repeatedly centrifuged and washed with pure water. Finally, the functionalized NTs were dried in vacuum. The powder was then ridispersed in 8 ml of 5 mM phosphate buffer at pH = 7 and the ionic self-assembly procedure was repeated by adding a H_2TPPS^{4-} solution (650 μM). Porphyrin molecules adsorb on the uncovered surface of the inorganic NTs and, after saturating it with ca. 5 ml of solution, they start to confer to the liquid a reddish color. The hybrid composite NTs were centrifuged and washed with water and finally dried in vacuum.

TEM observations. A JEOL JEM-1220 operating at 120 kV was used to image the HNTs. TEM samples were prepared by dispersing a few milligrams of the compounds in 2 ml of distilled water and dropping 3 μl of solution on carbon-coated copper-grids.

Optical characterization. Optical absorption spectra were recorded by a Varian Cary 50 spectrometer at normal incidence in dual beam mode, with a spectral resolution of 1 nm. For liquid samples the optical path was 0.6 cm. Typically, 0.75 mg of HNTs were dispersed in 2 ml of 10 mM acetate buffer at pH 6.5. The dispersion pH was lowered down to 2.5 by adding up to 260 µl of HCl 0.1 M. Photoluminescence (PL) spectra were detected by nitrogen-cooled CCD coupled with a double monochromator Triax-190 (Horiba Jobin-Yvon) with a spectral resolution of 0.5 nm. As light source a EPL-405 Edimburgh picosecond laser (pulse width) 150 ps has been employed. To monitor the FluoroMags response to acidity in PBS, the pH was lowered 2.5 by adding HCl 0.1 M. Time-resolved PL has been recorded with a Edimburgh FLS 980 spectrofluorometer. Fluorescence imaging and confocal PL measurements have been performed with an inverted fluorescence confocal microscope Nikon C1 coupled to a Canon 400D camera or to the nitrogen cooled CCD described above. Time resolved signal has been recorded in photon-counting mode using a Hamamatsu R943-02 photomultiplier connected to an Ortec 9353 multichannel scaler and to a Cornerstone monochromator.

Magnetic Relaxivity Measurements. A 0.5 T Bruker Minispec mq20 broadband spectrometer with ^{1}H Larmor frequency of 19.65 MHz was used for magnetic relaxometry in this work. All experiments were performed at 303 K (29.85 °C)±0.1 K temperature, obtained with BVT3000 Eurotherm nitrogen gas thermal apparatus. Dilution samples were prepared outside the NMR tube, and then 150 µL of each solution was inserted in a 10 mm o.d. tube, positioned in the magnet with the sample in the volume of maximum homogeneity of the B_0 and B_1 fields. All the samples were thermalized for 10 minutes before performing any experiment. For the $\pi/2$ and π, the pulse lengths were set to 2.07 µs and 4.15 µs respectively. A good signal to noise ratio was obtained within a few scans, but due to the analytical nature of this work, each sample was measured with 128 scans during CPMG experiments, and 64 scans per point during saturation recovery experiments. For $T_2 = (R_2)^{-1}$ measurement, we make use of Carr Purcell Meiboom Gill (CPMG) pulse sequence with parameters optimized for analytical use at low field.[70] This sequence consists of a first 90° pulse followed by a train of equally spaced 180° pulses. The signal is measured in the midpoint between each pair of 180° pulses and the obtained decay curve is fitted with a single exponential. For $T_1=(R_1)^{-1}$, we implemented saturation recovery sequence,[72] a sequence composed by a pulse train that is optimized for defocusing the magnetization of the sample.

Longitudinal magnetization is then measured using a single π/2 pulse after a set waiting time, and the time dependent recovery is fitted with a single exponential.

Ex-vivo Magnetic Resonance Imaging. An *ex vivo* tissue experiment was performed injecting 10^6 FluoroMags labeled 3T3 cells (labeling concentration: 25 μg/cm^2) into a chicken breast for MRI visualization. Images were obtained using a 4.7-T spectrometer (Burker, Koo Wee Rup, VIC, Australia) equipped with an in-house made surface coil. Single sagittal, coronal and transversal images were obtained by fast gradient-echo sequence to localize the subsequent T2-weighted transverse images, as measured by a standard turbo spin-echo sequence. Sequence parameters used were: repetition time (TR) = 2000 ms, effective echo time (TE) = 42.5 ms, turbo factor = 4, number of acquisitions (AC) = 16, field of view (FOV) = 3.5 cm, matrix 256 × 256, slice thickness 0.5 mm, slice separation 1 mm. Two sets of interleaved transversal images were measured to cover the whole muscle.

Cell viability and staining characterization of murine fibroblast cell line. NIH/3T3 mouse embryo fibroblast cells (ATCC® CRL-1658™) were thawed and plated on cell culture dish in DMEM high glucose (Gibco, Thermo Fisher Scientific; Waltham, Massachusetts, USA) supplemented with 10% fetal bovine serum (FBS) (Gibco, Thermo Fisher Scientific; Waltham, Massachusetts, USA) for 48 hours before use. For immunofluorescence experiments, NIH/3T3 cells were plated in 12 multiwell plates at a density of 5×10^4 cells/well and visualised by an inverted fluorescence microscope (Leica DMIRE2; Leica Microsystems Germany). Before seeding, cells were stained with PKH Green Kit (PKH67GL, Sigma-Aldrich; St. Louise, Missouri, USA), following the producer protocol. FluoroMags labeled NIH/3T3 cells were stained with calcein-AM (Live Dead cell viability kit, Molecular Probes, Thermo Fisher Scientific; Waltham, Massachusetts, USA), and imaged with fluorescence inverted microscope for viability assessment. Nuclei were counterstained with 2'-[4-ethoxyphenyl]-5-[4-methyl-1-piperazinyl]-2,5'-bi-1H-benzimidazole trihydrochloride trihydrate (1:2000 33342 Hoechst, Sigma-Aldrich; St. Louise, Missouri, USA). Acidosis was generated *via* media pH adjustment from pH 7.4 to pH 4.0 by HCl. Prussian Blue staining of cells was performed to determine the FluoroMags presence within cells throughout pH decrease.[51] Nuclei were counterstained by Nuclear Fast Red histological staining. For pH sensitive fluorescence FACS evaluation, $2x10^5$ FluoroMags labeled (25 μg cm^{-1}) NIH/3T3 were trypsinized and resuspended in 100 μl of PBS in flow cytometry tubes. pH decrease was

forced by sequentially adding HCl to set from pH 7.4 to 5. NIH/3T3 unlabeled cells were used as control. Cells were analyzed throughout a BD FACSAria SORP cell sorter (BD, Becton Dickinson; Franklin Lakes, New Jersey, USA) equipped with 5 lasers. In particular, a laser at 405 nm was used to excite cells. FluoroMags signal was collected using BV650 emission filter at 670/30nm (mirror 630LP). Dot plots and cytometry statistics were obtained using FlowJo software (i.e. percentage of FluoroMags positive population, median of fluorescence intensity, FSC-forward light scatter, and SSC-side scatter). Viable cells were manually gated on the basis of cell size and granularity. Graphs and statistical difference data were performed using GraphPad Software. FACS analysis was performed three times for each pH conditions. For setting the gates for positive events, unlabeled cells were used at pH 5 and pH 7 as control (data not shown).

MTT viability test. For proliferation experiments, NIH/3T3 cells were seeded in a 96 multiwell at a density of 3×10^3 cells/well in triplicate; after 24 hours nanoparticles were added to the cell medium at different concentrations: 200, 100, 50 and 25 μg cm^{-1}. MTT test was performed after 24 hours of labeling (Methylthiazolyldiphenyl-tetrazolium bromide, Sigma-Aldrich; St. Louise, Missouri, USA). A 50 μg/ml MTT solution was added to the samples; after 4 hours of incubation at 37°C the medium was removed, the converted dye solubilised with DMSO (dimethylsulfoxide, Sigma-Aldrich; St. Louise, Missouri, USA) and the absorbance measured at 560 nm (GloMax Discover, Promega; Fitchburg, Wisconsin, USA). Cells in growth medium were used as control.

Localization of lysosomal compartment. In order to determine the specific intracellular localization of FluoroMags, we have performed lysosome studies in a cell model of tumour throughout LysoTracker Green DND-26 (Thermo Fisher Scientific; Waltham, Massachusetts, USA) staining of human glioblastoma (GBM) derived adherent cells. All of the tumor clinical biopsies were collected from surgery resections of patients after informed consent, according to the guidelines of the Committee on the Use of human Subjects in Research of the Policlinico Hospital of Milano. Cells were isolated from human tumor processed immediately after surgery. Biopsies were treated as previously described.[73, 74] GBM derived adherent cells were cultured in 6-wells tissue culture plates in Dulbecco's modified Eagle's medium (DMEM)/F-12 medium (1:1) supplemented with 10% fetal bovine serum (FBS, Gibco). Cells adhered to the plastic and gradually formed a homogeneous monolayer composed of elongated

fibroblast-like cells. Growth medium was changed every two days until the cells reached 80% of confluence. Cells were then trypsined and re-plated into 8 wells chamber slides at a density of $10x10^3$/wells. LysoTracker Green DND-26 was perfomed according to manufacturer's instructions. Briefly, cells were washed once with PBS and incubated with 50nM of staining solution in growth medium for 30 minutes at 37°C. Hoechst (1:2000; Sigma-Aldrich; St. Louise, Missouri, USA) was used for nuclei counterstaining. Afterwards cells were washed with PBS and imaged live with a Leica DMi8 i fluorescent microscope (Leica, Germany).

Human Glioblastoma (GBM) derived cell characterization, hypoxia and soft-AGAR assay. Cells were isolated from human glioblastoma processed immediately after surgery. Cells were plated into untreated 6-well tissue culture plates (Nunc, Roskilde, Denmark) in Dulbecco's modified Eagle's medium (DMEM)/F-12 medium (1:1) containing of 20 ng/ml human recombinant EGF (Sigma-Aldrich) and 10 ng/ml human recombinant fibroblast growth factor (FGF2, Sigma-Aldrich), and labelled for 24 hours with FluoroMags at 25 μg cm^{-1} concentration. In these culture medium conditions, cells rapidly grew as neurospheres (GBM-NSs). The GBM-NSs were tested for their neural potential in differentiation medium. In these experiments the floating spheres were harvested, dissociated, and plated on collagen-coated wells in NeuroCult NS-A Basal medium (Stem Cell Technologies) added with 10% neurocult NS-A differentiation supplements (Gibco-BRL, Grand Island, NY) and cultured for 3 weeks. Immunocytochemistry on differentiated tumor cells was performed fixing cells with 4% paraformaldehyde and staining with antibodies against nestin (1:50; BD), GFAP (1:300, Sigma) and β-tubulin III (1:50 Sigma). For acidosis induced by inadequate oxygen levels, after 4 days neuropsheres were collected, mechanically dissociated and single cells incubated either in normoxia (20% O_2 and 5%CO_2) or hypoxia (1% O_2 and 5%CO2) conditions. For HCl-induced acidosis, neurospheres maintained in normoxia condition (20% O_2 and 5%CO_2) were exposed to decreasing pHs, as previously described. FluoroMags signal was detected by fluorescence microscopy, and measured by a microplate spectrophotometer (Exc. 405 nm, Em. 645nm, GLOMAX Promega). Soft-agar assay was performed as already described.[75, 76] Briefly, 2.5% agarose stock was made in 1X PBS. The bottom, 0.5% agar support was prepared in DMEM/F-12 medium 2×10^5 labeled GBM derived cells were harvested, washed and mixed with the top-agarose suspension at a final concentration of 0.3–0.33%, which was then layered

onto the bottom agar in 12 multiwell plates. The agar plates were incubated at 37°C for 21 days. Medium was changed every 3 days. Detection of FluoroMags fluorescence was performed at different experimental days.

***In vivo* experimental procedures.** Throughout the experiments, mice were handled in agreement with guidelines conforming the Italian regulations for the animal uses for scientific purposes (DL. Vo 116/92). Procedures were approved by Ethical Committees for Animal Experimentation of the IRCCS Policlinico di Milano and of the Ospedale Policlinico San Martino di Genova and by Italian Ministry of Health. During the in vivo procedures and MR imaging, mice were anesthetized by intraperitoneally injections of Zoletil (150mg/kg) or fentanyl/midazolam/medetomidine (0.05/5/0.5 mg/kg). Euthanasia was performed by cervical dislocation.

Evaluation of tumorigenicity by orthotopic injection in nude mice. Tumorigenicity was determined by stereotactical injection of 10^5 human GBM-NSs into the right forebrain (2 mm lateral and 1 mm anterior to bregma, at a 2 mm depth from the skull surface) of two months-old *nu/nu* mice as previously described. Animals were sacrificed immediately (n=3) and 90 days after transplantation. During all the experiments period, animals were carefully monitored for the occurrence of any side effects. All brains were removed and frozen in liquid nitrogen–cooled isopentane. Cryostat sections from frozen tissues embedded in ornithine carbamyl transferase (OCT) were cut into 10 µm serial sections. Slides were incubated with antibodies anti-lamin A/C (1:100; Novocastra), anti-human nestin (1:50; BD), anti-human GFAP (1:300, Sigma Aldrich). Primary antibodies were diluted in PBS containing 1% horse serum and then incubated for 2h at room temperature. The sections were rinsed in PBS and incubated with corresponding secondary antibodies Alexa Fluor 488 or Alexa Fluor 594, (1:200, Molecular Probes), for 30 min a room temperature. Cell nuclei were stained with 4',6-diamidino-2-phenylindole (DAPI), and sections were mounted with ProLong anti-Fade (Molecular Probes). For all immunostaining, control reactions were done omitting the primary antibody, which was substituted by non-immune serum. Sections were examined under a Leica TCS-SP2 confocal microscope by Leica Confocal Software, and under Leica fluorescent microscope DMIRE2 by Q-Fluoro Software.

***In-vivo* Magnetic Resonance Imaging.** In vivo MR images have been acquired using a horizontal 7 T MRI scanner (Bruker BioSpec 70/30 USR, Bruker, Germany) equipped with a BGA12-S gradient coil

with a diameter of 12 cm and a maximum gradient strength of 440 mT/m. A mouse brain dedicated surface radio frequency (RF) coil for reception and a volume RF coil for transmission have been used. The distribution of the GBM-NSs was monitored using the paramagnetic properties of the ferro-magnetic nano-particles. Sagittal, coronal and axial images were obtained by a Turbo RARE sequence (TE = 39 ms, TR = 3.5 s, RARE factor = 8, slice thickness 0.7 mm, FOV= 3 cm × 2 cm, 256 · 256 matrix) to localize the subsequent T2-weighted (TE = 54 ms, TR = 3,5 s) and Flash T2*-weighted (TE = 7 ms, TR = 0.7 s) axial images acquired with the same geometry (slice thickness = 0.6 mm, FOV = 1.8 cm × 1.8 cm, 200 × 200 matrix). The MRI protocol includes a Gradient-Echo T2*-weighted sequences, and multi-echo T2*-weighted sequences for the quantification of the T2* of the tissue.

Evaluation of BBB penetrating ability of FluoroMags. Glioma animal model was obtained by stereotactical injections of 10^5 human GBM tumor initiating cells engineered with pCAG:DsRed and pCAG:mGFP-Gluc into the left forebrain (1.5 mm lateral and 1 mm anterior to bregma, at a 2.5 mm depth from the skull surface) of Nod/Scid mice.[36, 68] This way, the tumor size and the intracranial growth of gliomas were easily detectable by fluorescence microscopy as luciferase Ds-Red positive areas (Supplementary Fig.5). Excitation and emission maxima are 554 and 586 nm, respectively, with no overlap with FluoroMags absorption spectrum. Ds-Red positive cells are visualized in Fig. 8 using a green pseudocolor. N=4 Nod/Scid mice were systemically infused in tail vein with 500 μg of FluoroMags in 100 μl of PBS. N=5 untreated animals were used as controls. Animals were sacrificed after 7 days with an overdose of ketamine/xylazine and transcardiacal perfused with PFA 4% Brain tissues were removed, cryoprotected in 20% sucrose, embedded in OCT and frozen in dry ice. 10 μm serial sections from frozen tissues were then cut to investigate the FluoroMag presence within brains.

Acknowledgements

A. M. acknowledges support from Università degli Studi Milano-Bicocca (grant n°2016 ATESP0052). C.V. and Y.T. acknowledge support from Associazione “Amici del Centro Dino Ferrari” and from Fondazione Roby ONLUS.

References

[1] S. Thomas, N. Kalarikkal, A. Manuel Stephan, B. Raneesh, A. K. Haghi, *Advanced Nanomaterials: Synthesis, Properties, and Applications*. Apple Academic Press, 2014.

[2] T. Maldiney, A. Bessière, J. Seguin, E. Teston, S. K. Sharma, B. Viana, A. J. J. Bos, P. Dorenbos, M. Bessodes, D. Gourier, D. Scherman, C. Richard, *Nat. Mater.* **2014,** *13*, 418.

[3] I. Villa, A. Vedda, I. X. Cantarelli, M. Pedroni, F. Piccinelli, M. Bettinelli, A. Speghini, M. Quintanilla, F. Vetrone, U. Rocha, C. Jacinto, E. Carrasco, F. S. Rodríguez, Á. Juarranz, B. del Rosal, D. H. Ortgies, P.H. Gonzalez, J. G. Solé, D. J. García, *Nano Res.* **2014,** *8*, 649.

[4] E.-K. Lim, T. Kim, S. Paik, S. Haam, Y.-M. Huh, K. Lee, *Chem. Rev.* **2015,** *115*, 327.

[5] Q. Le Trequesser, H. Seznec, M. H. Delville, *Nanotechnol. Rev.* **2013**, *2*, 125.

[6] D. H. Ortgies, L. de la Cueva, B. del Rosal, F. Sanz-Rodríguez, N. Fernández, M. C. Iglesias-de la Cruz, G. Salas, D. Cabrera, F. J. Teran, D. Jaque, E. Martín Rodríguez, *ACS Applied Materials & Interfaces* **2016,** *8*, 1406.

[7] S. Bouccara, G. Sitbon, A. Fragola, V. Loriette, N. Lequeux, T. Pons, *Curr. Opin. Biotechnol.* **2015,** *34*, 65.

[8] J. H. Park, G. von Maltzahn, E. Ruoslahti, S. N. Bhatia, M. J. Sailor, *Angew. Chem. Int. Ed.* **2008,** *47*, 7284.

[9] O. Chen, L. Riedemann, F. Etoc, H. Herrmann, M. Coppey, M. Barch, C. T. Farrar, J. Zhao, O. T. Bruns, H. Wei, P. Guo, J. Cui, R. Jensen, Y. Chen, D. K. Harris, J. M. Cordero, Z. Wang, A. Jasanoff, D. Fukumura, R. Reimer, M. Dahan, R. K. Jain, M. G. Bawendi, *Nat. Commun.* **2014,** *5*, 5093.

[10] D. Le Sage, K. Arai, D. R. Glenn, S. J DeVience, L. M. Pham, L. Rahn-Lee, M. D. Lukin, A. Yacoby, A. Komeili, R. L. Walsworth, *Nature* **2013,** *496*, 486.

[11] O. T. Bruns, H. Ittrich, K. Peldschus, M. G. Kaul, U. I. Tromsdorf, J. Lauterwasser, M. S. Nikolic, B. Mollwitz, M. Merkel, N. C. Bigall, S. Sapra, R. Reimer, H. Hohenberg, H. Weller, A. Eychmuller, G. Adam, U. Beisiegel, J. Heeren, *Nat. Nano.* **2009,** *4*, 193.

[12] S. Corr, Y. Rakovich, Y. Gun'ko, *Nanoscale Res. Lett.* **2008,** *3*, 87.

[13] J. Kim, H. S. Kim, N. Lee, T. Kim, H. Kim, T. Yu, I. C. Song, W. K. Moon, T. Hyeon, *Angew. Chem. Int. Ed.* **2008,** *47*, 8438.

[14] H. Gu, R. Zheng, X. Zhang, B. Xu, *J. Am. Chem. Soc.* **2004,** *126*, 5664.

[15] J. Gao, W. Zhang, P. Huang, B. Zhang, X. Zhang, B. Xu, *J. Am. Chem. Soc.* **2008,** *130*, 3710.

[16] G. Ruan, G. Vieira, T. Henighan, A. Chen, D. Thakur, R. Sooryakumar, J. O. Winter, *Nano Lett.* **2010,** *10*, 2220.

[17] Z. Lu, C. Gao, Q. Zhang, M. Chi, J. Y. Howe, Y. Yin, *Nano Lett.* **2011,** *11*, 3404.

[18] H. M. Kim, H. Lee, K .S. Hong, M. Y. Cho, M. H. Sung, H. Poo, Y. T. Lim, *ACS Nano* **2011,** *5*, 8230.

[19] J. R. Casey, S. Grinstein, J. Orlowski, *Nat. Rev. Mol. Cell Bio.* **2009,** *11*, 50.

[20] H. J. Adrogue, N. E. Madias, *New Engl. J. Med.* **1998,** *338*, 26.

[21] S. Grinstein, C. J. Swallow, O. D. Rotstein, *Clin. Biochem.* **1991,** *24*, 241.

[22] B. G. Wouters, M. Koritzinsky, *Nat. Rev. Cancer* **2008,** *8*, 851.

[23] O. Warburg, F. Wind, E. Negelein, *J. Gen. Physiol.* **1927,** *8*, 519.

[24] A. I. Hashim, X. Zhang, J. W. Wojtkowiak, G. V. Martinez, R. J. Gillies, *NMR Biomed.* **2011,** *24*, 582.

[25] M. Damaghi, J. W. Wojtkowiak, R. J. Gillies, *Front. Physiol.* **2013,** *4*, 370.

[26] R. J. Gillies, N. Raghunand, M. L. Garcia-Martin, R. A. Gatenby, *IEEE Eng. Med. Biol. Mag.* **2004,** *23*, 57.

[27] N. Raghunand, X. He, R. van Sluis, B. Mahoney, B. Baggett, C. W. Taylor, G. Paine-Murrieta, D. Roe, Z. M. Bhujwalla, R. J. Gillies, *Br. J. Cancer.* **1999,** *80*, 1005.

[28] W. A. Banks, *Nat. Rev. Drug Discov.* **2016,** *15*, 275.

[29] L. B. de Paula, F. L. Primo, A. C. Tedesco, *Biophys. Rev.* **2017,** *9*, 761.

[30] S. Barua, S. Mitragotri, *Nano Today* **2014**, 9, 223.

[31] G. De Luca, A. Romeo, V. Villari, N. Micali, I. Foltran, E. Foresti, I. G. Lesci, N. Roveri, T. Zuccheri, L. M. Scolaro, *J. Am. Chem. Soc.* **2009,** *131*, 6920.

[32] E. Gazzano, F. Turci, E. Foresti, M. G. Putzu, E. Aldieri, F. Silvagno, I. G. Lesci, M. Tomatis, C. Riganti, C. Romano, B. Fubini, N. Roveri, D. Ghigo, *Chem. Res. Toxicol.* **2007,** *20*, 380.

[34] S. Marchesan, K. Kostarelos, A. Bianco, M. Prato, *Materials Today* **2015,** *18*, 12.

[35] J. J. Lochhead, R. G. Thorne, *Adv. Drug Deliv. Rev.* **2012,** *64*, 614.

[36] M. J. Larsen, R. D. Martin, E. M. Byrne, *Curr. Top. Med. Chem.* **2014,** *14*, 1148.

[37] F. Alessandrini, D. Ceresa, I. Appolloni, D. Marubbi, P. Malatesta, *J. Cancer* **2016,** *7*, 1791.

[38] F. A. Gallagher, M. I. Kettunen, S. E. Day, D.-E. Hu, J. H. Ardenkjær-Larsen, R. Zandt, P. R. Jensen, M. Karlsson, K. Golman, M. H. Lerche, K. M. Brindle, *Nature* **2008,** *453*, 940.

[39] I. G. Lesci, G. Balducci, F. Pierini, F. Soavi, N. Roveri, *Microporous Mesoporous Mater.* **2014,** *197*, 8.

[40] Y. Zakrevskyy, J. Stumpe, C. F. J. Faul, *Adv. Mater.* **2006,** *18*, 2133.

[41] L. Li, E. Beniash, E. R. Zubarev, W. Xiang, B. M. Rabatic, G. Zhang, S. I. Stupp, *Nat. Mater.* **2003,** *2*, 689.

[42] A. Monguzzi, I. G. Lesci, G. C. Capitani, N. Santo, N. Roveri, M. Campione, *Phys. Chem. Chem. Phys.* **2014,** *16*, 2491.

[43] M. Gouterman, G. H. Wagnière, L. C. Snyder, *J. Mol. Spectrosc.* **1963,** *11*, 108.

[44] A. Kaibara, G. Matsumara, *Handbook of porphyrins : chemistry, properties, and applications*. Nova Science Publishers: Hauppauge, N.Y., 2011.

[44] J. R. Lakowicz. *Principles of Fluorescence* (Springer Science, LLC, Boston, MA, 2006).

[45] U. I. Tromsdorf, N. C. Bigall, M. C. Kaul, O. T. Bruns, M. S. Nikolic, B. Mollwitz, R. A. Sperling, R. Reimer, H. Hohenberg, W. J. Parak, S. Förster, U. Beisiegel, G. Adam, H. Weller, *Nano Lett.* **2007,** *7*, 2422.

[46] Y. Gossuin, P. Gillis, A. Hocq, Q. L. Vuong, A. Roch, *Wiley Interdiscip. Rev. Nanomed. Nanobiotechnol.* **2009**, *1*, 299.

[47] J. Kapuscinski, *Biotech. Histochem.* **1995,** *70*, 220.

[48] A. Muthuraja, S. Kalainathan, *Mater. Res. Innov.* **2016,** *20*, 358.

[49] T. Mosmann, *J. Immunol. Methods* **1983,** *65*, 55.

[50] T. A. Thompson, *Methods Mol. Med.* **1999,** *22*, 145.

[51] R. A. Petros, J. M. DeSimone, *Nat. Rev. Drug Discov.* **2010,** *9*, 615.

[52] P. Jendelová, V. Herynek, J. De Croos, K. Glogarová, B. Andersson, M. Hájek, E. Syková, *Magn. Reson. Med.* **2003,** *50*, 767.

[53] T. A. Kelf, V. K. Sreenivasan, J. Sun, E. J. Kim, E. M. Goldys, A. V. Zvyagin, *Nanotechnology* **2010,** *21*, 285105.

[54] C. D. Bortner, J. A. Cidlowski, *Cell Death Differ.* **2002,** *9*, 1307.

[55] Z. Chu, S. Zhang, B. Zhang, C. Zhang, C.-Y. Fang, I. Rehor, P. Cigler, H.-C. Chang, G. Lin, R. Liu, Q. Li, *Sci. Rep.* **2014,** *4*, 4495.

[56] D. B. Gürsel, J. B. Shin, J.-K. Burkhardt, K. Kesavabhotla, C. D. Schlaff, J. A. Boockvar, *Cancers* **2011,** *3*, 2655.

[57] J. Chiche, M. C. Brahimi-Horn, J. Pouyssegur, *J. Cell. Mol. Med.* **2010,** *14*, 771.

[58] R. L. Jensen, *J. Neurooncol.* **2009,** *92*, 317.

[59] J. T. Chi, Z. Wang, D. S. Nuyten, E. H. Rodriguez, M. E. Schaner, A. Salim, Y. Wang, G. B. Kristensen, A. Helland, A. L. Borresen-Dale, A. Giaccia, M. T. Longaker, T. Hastie, G. P. Yang, M. J. van de Vijver, P. O. Brown, *PLoS Med.* **2006,** *3*, e47.

[60] K. L. Bennewith, S. Dedhar, *BMC Cancer* **2011,** *11*, 504.

[61] A. B. Hjelmeland, Q. Wu, J. M. Heddleston, G. S. Choudhary, J. MacSwords, J. D. Lathia, R. McLendon, D. Lindner, A. Sloan, J. N. Rich, *Cell Death Differ.* **2011,** *18*, 829.

[62] C. F. Gao, Q. Xie, Y. L. Su, J. Koeman, S. K. Khoo, M. Gustafson, B. S. Knudsen, R. Hay, N. Shinomiya, G. F. Vande Woude, *Proc. Natl. Acad. Sci. USA* **2005,** *102*, 10528.

[63] A. K. Kamat, M. Rocchi, D. I. Smith, O. J. Miller, *Somat. Cell Mol. Genet.* **1993,** *19*, 203.

[64] R. Galli, E. Binda, U. Orfanelli, B. Cipelletti, A. Gritti, S. De Vitis, R. Fiocco, C. Foroni, F. Dimeco, A. L. Vescovi, *Cancer Res.* **2004,** *64*, 7011.

[65] H. D. Hemmati, I. Nakano, J. A. Lazareff, M. Masterman-Smith, D. H. Geschwind, M. Bronner-Fraser, H. I. Kornblum, *Proc. Natl. Acad. Sci. USA* **2003,** *100*, 15178.

[66] T. N. Ignatova, V. G. Kukekov, E. D. Laywell, O. N. Suslov, F. D. Vrionis, D. A. Steindler, *Glia* **2002,** *39*, 193.

[67] S. K. Singh, C. Hawkins, I. D. Clarke, J. A. Squire, J. Bayani, T. Hide, R. M. Henkelman, M. D. Cusimano, P, B. Dirks, *Nature* **2004,** *432*, 396.

[68] I. Appolloni, M. Barilari, S. Caviglia, E. Gambini, E. Reisoli, P. Malatesta, *Oncogene* **2014,** *34*, 1991.

[69] S. Sun, H. Zeng, *J. Am. Chem. Soc.* **2002,** *124*, 8204.

[70] S. Dey, K. Mohanta, A. J. Pal, *Langmuir* **2010,** *26*, 9627.

[71] M. Mauri, M. K. Dibbanti, M. Calzavara, L. Mauri, R. Simonutti, V. Causin, *Anal. Methods* **2013,** *5*, 4336.

[72] M. Mauri, Y. Thomann, H. Schneider, K. Saalwächter, *Solid State Nucl. Mag. Reson.* **2008,** *34*, 125.

[73] A. Gritti, E. A. Parati, L. Cova, P. Frolichsthal, R. Galli, E. Wanke, L. Faravelli, D. J. Morassutti, F. Roisen, D. D. Nickel, A. L. Vescovi, *J. Neurosci.* **1996,** *16*, 1091.

[74] B. A. Reynolds, S. Weiss, *Science* **1992,** *255*, 1707.

[75] P. Kunapuli, K. S. Chitta, J. K. Cowell, *Oncogene* **2003,** *22*, 3985.

[76] F. Colleoni, M. Belicchi, P. Razini, M. Meregalli, R. Galli, S. Mazzoleni, S. Brunelli, M. Di Segni, D. Coviello, M. Baccarin, B. Pollo, N. Bresolin, L. Bello, L. Conti, Y. Torrente, *J. Stem Cell Res. Ther.* **2015,** *1*, 00006.